

# Journal of Materials Chemistry A

Accepted Manuscript



This is an *Accepted Manuscript*, which has been through the Royal Society of Chemistry peer review process and has been accepted for publication.

*Accepted Manuscripts* are published online shortly after acceptance, before technical editing, formatting and proof reading. Using this free service, authors can make their results available to the community, in citable form, before we publish the edited article. We will replace this *Accepted Manuscript* with the edited and formatted *Advance Article* as soon as it is available.

You can find more information about *Accepted Manuscripts* in the [Information for Authors](#).

Please note that technical editing may introduce minor changes to the text and/or graphics, which may alter content. The journal's standard [Terms & Conditions](#) and the [Ethical guidelines](#) still apply. In no event shall the Royal Society of Chemistry be held responsible for any errors or omissions in this *Accepted Manuscript* or any consequences arising from the use of any information it contains.

## ARTICLE

## Manipulation of Cuprous Oxide Surfaces for Improving Their Photocatalytic Activity

Cite this: DOI: 10.1039/x0xx00000x

Sanghwa Yoon,<sup>a</sup> Misung Kim,<sup>b,c</sup> In-Soo Kim,<sup>c</sup> Jae-Hong Lim<sup>b,†</sup> and Bongyoung Yoo<sup>a,†</sup>Received 00th January 2012,  
Accepted 00th January 2012

DOI: 10.1039/x0xx00000x

www.rsc.org/

Manipulating the surface characteristics of metal oxide electrodes allows the properties of the interface between the electrodes and the electrolyte to be controlled and can lead to improvements in both the efficiency and reliability of the electrodes. In this study, the facets exposed on the surfaces of Cu<sub>2</sub>O photoelectrodes were manipulated by controlling the pH of the bath during Cu<sub>2</sub>O film electrodeposition. The Cu<sub>2</sub>O film with (100)-type facets, deposited at a bath pH of 12, produced a photocurrent 19 times higher than that of the film deposited at pH 8.3 and possessing (111) facets. In addition, inverse-opal-structured Cu<sub>2</sub>O films were electrodeposited in alkali solutions using templates of polystyrene beads; these films exhibited even higher photocatalytic activities than the planar ones. The templated, three-dimensional (3D) Cu<sub>2</sub>O film deposited at pH 12 produced a photocurrent 2.14 times higher than that generated by the planar Cu<sub>2</sub>O film deposited at the same pH; this was a result of the greater surface area and higher light absorption of the 3D film.

### Introduction

In recent years, increasing effort is being devoted to the generation of energy using thermoelectric sources, water, wind, solar radiation, and hydrogen, given the diminishing reserves of fossil fuels and the associated CO<sub>2</sub> greenhouse effect. The combustion of hydrogen in fuel cells ( $\text{H}_2 + 1/2 \text{O}_2 \rightarrow \text{H}_2\text{O} + \text{energy}$ ) shows particular promise as an alternative energy generation technique. Currently, hydrogen is mostly produced from natural gas by steam methane reforming, which yields a large amount of hydrogen at low cost. However, the production of hydrogen from natural gas is not environmentally friendly because a large amount of CO<sub>2</sub> is produced as well. In contrast, the photoelectrochemical (PEC) splitting of water using sunlight is an environmentally friendly method for producing hydrogen and oxygen without producing any undesired reactants/pollutants.

A PEC cell consists of two semiconductor photoelectrodes in an aqueous electrolyte, and its operation is based on the electrochemical interaction between the photoelectrodes and the electrolyte.<sup>1, 2</sup> Controlling the facets exposed on the surfaces of the electrodes is important for enhancing the performance of the electrodes during PEC reactions. This is because the facets on the surface of an electrode determine the interfacial area between the electrode and the electrolyte, the diffusion length of the minority carriers, and the optical absorption depth, among other parameters.<sup>3-8</sup> In particular, the facet type determines the barrier height at the electrode-electrolyte interface.

Because every facet has a unique atomic arrangement, the type of facets present could determine the adsorption behaviour of ions or molecules on the electrode surface, resulting in a variety of different surface reactions in a PEC cell.<sup>9</sup> In addition, increasing the facet surface area is also important because it can increase the rate of the surface reactions as well as enhance overall light absorption. To fabricate such faceted surfaces, various nanostructures have been suggested, such as nanoplates,<sup>10</sup> nanoribbons,<sup>11</sup> nanotubes,<sup>3, 12</sup> and fullerene-like nanoparticles.<sup>13, 14</sup> Cuprous oxide (Cu<sub>2</sub>O) is a promising material candidate for the photoelectrodes in PEC cells<sup>4, 15-17</sup> and the p-type absorber layer of solar cells<sup>5, 7, 18-20</sup> because of its direct band gap size (2.1 eV) and high absorption coefficient. In addition, its conduction band lies above the hydrogen evolution potential, and it is abundant in nature. For example, a highly active and stable photocathode consisting of Cu<sub>2</sub>O films exhibited photocurrents of up to  $-7.6 \text{ mA/cm}^2$  and produced  $75 \pm 10 \mu\text{L}$  of hydrogen after a total charge of 0.58 C passed through it at 0 V vs. a reversible hydrogen electrode or RHE).<sup>4</sup>

In addition, Cu<sub>2</sub>O/ZnO heterojunctions have been employed in solar cells to achieve conversion efficiencies of 1.28%.<sup>20</sup> Even though Cu<sub>2</sub>O films have theoretical conversion efficiencies of 24% (solar energy into electricity) and 18% (solar energy into hydrogen), their actual conversion efficiencies are relatively low. One factor that negatively influences the performance of Cu<sub>2</sub>O-based solar cells is the mismatch between the minority-carrier diffusion length (which is small, 20–100 nm) and the light adsorption depth (which is large,  $\sim 10 \mu\text{m}$ ).<sup>5</sup>

Several methods for improving the activity and stability of  $\text{Cu}_2\text{O}$  surfaces have been investigated in order to address this problem. For instance, the activity of the polar  $\text{Cu}_2\text{O}$  {100} surfaces was found to be higher than that of the {111} surfaces; this was because the number of surface interactions with water molecules was greater in the case of the former surface. The {100} surfaces also exhibited higher carrier mobility as a result of the type of facets present on them.<sup>16</sup> On the other hand,  $\text{Cu}_2\text{O}$  tends to be unstable in electrolytes under irradiation because its reduction potential is lower than the potential required for hydrogen generation. The reductive decomposition of  $\text{Cu}_2\text{O}$  electrodes occurs primarily at the {100} surfaces.<sup>16, 21</sup> Therefore, manipulation of the electrodeposited  $\text{Cu}_2\text{O}$  film surfaces *via* control of the deposition parameters such as the bath pH, electrolyte concentration, and the metal salts present has been studied extensively.<sup>17, 21, 22</sup> However, the manipulation of  $\text{Cu}_2\text{O}$  film surfaces using templates with pattern features ranging in size from the angstrom scale to the micron scale has not yet been attempted.

In this study, we investigated the differences in photocurrent generated in  $\text{Cu}_2\text{O}$  films with surfaces having different types of facets. The films were fabricated using electrochemical deposition methods. The type of facets exposed on the  $\text{Cu}_2\text{O}$  films was controlled by controlling the pH of the electrolyte. As mentioned previously, the polarity of the exposed surface affects the interactions between the adsorbed electrolyte ions and the  $\text{Cu}_2\text{O}$  electrode and, in turn, determines the overall photocatalytic activity of the electrode. In addition, the effects of three-dimensional (3D)  $\text{Cu}_2\text{O}$  structures on the generation of photocurrent were studied. A 3D structure consisting of randomly exposed facets was synthesised using a template of polystyrene (PS) beads to increase the surface area and the light absorption. PS beads have been used widely as templates to fabricate periodic 3D structures that increase the surface area and light absorption of electrodes, thereby enhancing the photonic effect in dye-sensitised solar cells and GaAs-based optoelectronic devices.<sup>8, 23</sup>

## Results and discussion

The crystal orientation and morphology of electrodeposited  $\text{Cu}_2\text{O}$  films are affected by the bath pH.<sup>21</sup> Figure 1 shows field-emission scanning electron microscopy (FESEM) images of the  $\text{Cu}_2\text{O}$  thin films deposited at pH 12 and pH 8.3. To confirm the relationship between the bath pH and the crystal orientation, the samples were characterised using X-ray diffractometry (XRD), as well (Fig. S1 in the ESI). The  $\text{Cu}_2\text{O}$  film deposited at pH 12 exhibited (111) orientations only, and its grains appeared as triangular pyramids with exposed (100) facets (Fig. 1(a)). On the other hand, the film deposited at pH 8.3 exhibited both (111) and (100) orientations and mainly consisted of quadrangular pyramidal grains with exposed (111) facets (Fig. 1(b)).

The surface morphology is affected by the growth rate of the surface crystals. Because the number of oxygen atoms per unit area is different for the (100) and (111) surfaces, the facet structure is determined by the hydroxyl group concentration in the solution during deposition.<sup>21</sup> Also, the differences in the crystal orientations of

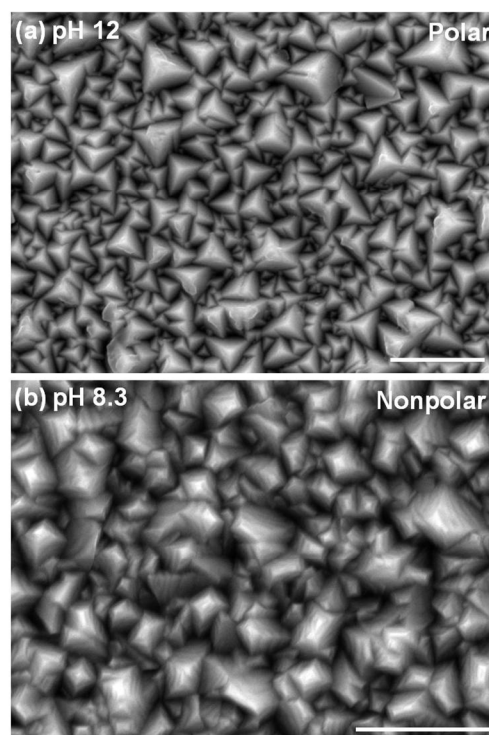


Figure 1. SEM images of  $\text{Cu}_2\text{O}$  films deposited on Au/Ti-coated Si substrates at bath pH values of (a) 12 and (b) 8.3. The scale bar is 2  $\mu\text{m}$ .

the  $\text{Cu}_2\text{O}$  films were caused by differences in the exchange current densities during deposition, as determined by the different pH values.<sup>26, 27</sup> Sower *et al.* investigated the stoichiometric termination of the surfaces of  $\text{Cu}_2\text{O}$  films deposited at pH values of 9 and 12. They found that the (111)  $\text{Cu}_2\text{O}$  surface deposited at pH 9 had a  $\text{Cu}^+$ -terminated layer when the initially deposited atoms were oxygen. On the other hand, the  $\text{Cu}_2\text{O}$  (100) surface deposited at pH 12 had  $\text{O}^{2-}$ -terminated layers. The type of terminating layer present significantly affects the stability of the  $\text{Cu}_2\text{O}$  films when they are used in PEC cells; the (111) surface is more stable than the (100) surface, which undergoes  $\text{H}^+$ -assisted reduction. However, the photocurrent generated in the  $\text{Cu}_2\text{O}$  film deposited at pH 12 was higher than that of the film deposited at pH 9 because of the  $\text{O}^{2-}$  sites produced by the  $\text{H}^+$ -assisted reduction of  $\text{Cu}_2\text{O}$  at the (100) surface.<sup>16</sup> This phenomenon was also observed in the present study.

The variations in photocurrent ( $I$ ) generated in the different  $\text{Cu}_2\text{O}$  films on a per-unit-area basis are shown in Fig. 2. The values of  $I$  in the polar  $\text{Cu}_2\text{O}$  film deposited at pH 12 was approximately 6 times higher than that of the nonpolar  $\text{Cu}_2\text{O}$  film deposited at pH 8.3 at a potential ( $V$ ) of  $-0.5$  V vs. Ag/AgCl (Fig. 3(a)). The “dark” current of the polar  $\text{Cu}_2\text{O}$  film with the  $\text{O}^{2-}$ -terminated surface was large; this indicates that the reduction of  $\text{Cu}_2\text{O}$  can occur under dark conditions. This phenomenon was accelerated in the case of the 3D films, which had larger surface areas and random surface profiles. The photoresponses of the films with respect to time ( $I$ - $t$  behaviour) were measured at  $V = -0.4$  V (vs. Ag/AgCl) using chopped illumination; the “ON” and “OFF” intervals were 20 s, each. The rise and fall of  $I$  corresponded well with the ON and OFF periods.

When the illumination was interrupted, the photocurrent dropped rapidly to near zero (the steady-state value). It then reverted to the original value when the light source was applied again. The transient photocurrent density of the polar 2D Cu<sub>2</sub>O film (deposited at pH 12) was less than  $-0.39 \text{ mA cm}^{-2}$ , whereas that of the nonpolar 2D Cu<sub>2</sub>O film (deposited at pH 8.3) was greater than  $-0.07 \text{ mA cm}^{-2}$ . The flat-band potential of polar Cu<sub>2</sub>O films terminated with {100} planes is usually higher than that of a similar nonpolar Cu<sub>2</sub>O films presenting {111} planes. This results in an increase in the rate of separation of the photogenerated electron-hole pairs on the face of the polar Cu<sub>2</sub>O films. Hence, the photocurrent generated in the film is also higher.<sup>9, 21</sup>

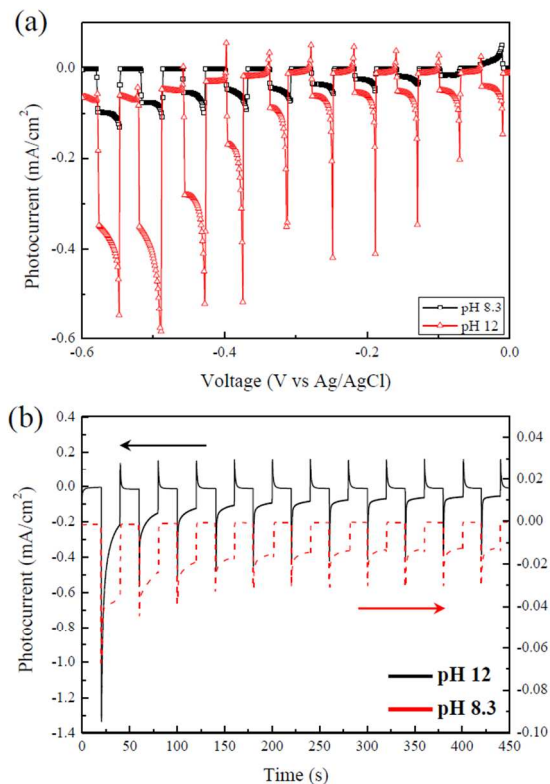


Figure 2 Photocurrent densities of the 2D Cu<sub>2</sub>O films deposited at pH levels of 8.3 and 12. (a) *I-V* characteristics for potentials in the range 0 V to  $-0.6 \text{ V}$  (vs. Ag/AgCl). (b) Time-resolved photoresponses in a  $0.5 \text{ M Na}_2\text{SO}_4$  solution at  $-0.4 \text{ V}$  (vs. Ag/AgCl).

The electrical transport properties, which are related to the carrier mobility, of the polar and nonpolar Cu<sub>2</sub>O films were determined by Hall effect measurements made in the van der Pauw configuration.<sup>17</sup> The electrical resistivity of the polar Cu<sub>2</sub>O film was  $1.15 \times 10^3 \Omega \text{ cm}$  under dark conditions, whereas that of the nonpolar Cu<sub>2</sub>O film was  $3.19 \times 10^4 \Omega \text{ cm}$ . In addition, the carrier concentrations of the polar and nonpolar Cu<sub>2</sub>O films were  $2.15 \times 10^{15}$  and  $8.59 \times 10^{14} \text{ cm}^{-3}$ , respectively, and their carrier mobilities were  $2.52$  and  $0.23 \text{ cm}^2 \text{ V}^{-1} \text{ s}^{-1}$ , respectively. It has been reported that the carrier concentration of electrodeposited Cu<sub>2</sub>O films depends on the metal deficiency/nonstoichiometry and that the carrier mobility is related to the Cu<sub>2</sub>O grain size.<sup>28</sup> Therefore, the large grain size ( $0.4\text{--}1.5 \mu\text{m}$ ) of the polar Cu<sub>2</sub>O film resulted in the film exhibiting high charge

carrier separation rate and carrier mobility; this, in turn, improved its photocurrent density and led to a higher photocurrent.

Figure 3 shows the PS bead template and the morphology of the 3D Cu<sub>2</sub>O films deposited using the template. It is clear from Fig. 3(a) that the PS beads do not form a periodic array. The inverse-opal-structured Cu<sub>2</sub>O films electrodeposited at pH 8.3 and 12 were both highly porous. However, they had nonpolar structures, indicating that their exposed facets consisted of randomly mixed Cu<sup>+</sup>- or O<sup>2-</sup>-terminated layers, as shown in Figs. 3(b) and (c). The orientation and growth direction of the Cu<sub>2</sub>O films were not affected by the PS beads. Although Cu<sub>2</sub>O grew over the PS bead template, we could still observe the {100} planes, which were similar to those of the 2D films (Fig. 3(d)). Furthermore, the XRD data (Fig. S2 in the ESI) indicate that the preferred crystal orientations in the 3D Cu<sub>2</sub>O films deposited at pH 8.3 and 12 were the same as those of the corresponding 2D films.

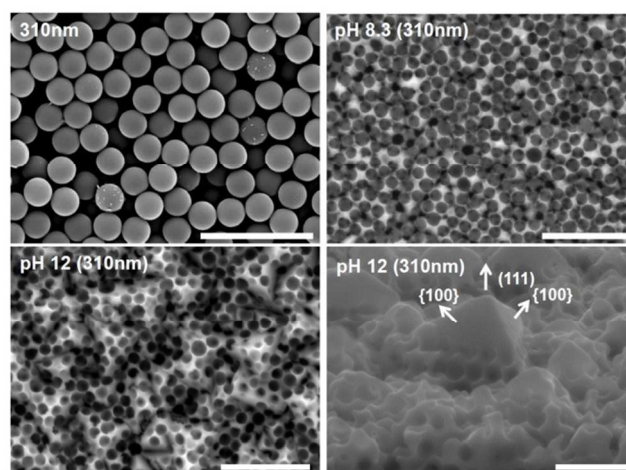


Figure 3. SEM images of (a) the template of PS beads 310 nm in diameter; (b), (c) the morphologies of the 3D Cu<sub>2</sub>O films deposited at pH 8.3 and pH 12, respectively; and (d) the cross-section of the 3D Cu<sub>2</sub>O film deposited at pH 12. The film in (d) also exhibited a (111) orientation. The scale bars are  $1 \mu\text{m}$ .

The room-temperature Raman and photoluminescence (PL) spectra of the 2D and 3D Cu<sub>2</sub>O films are shown in Fig. S3 in the ESI; these spectra further elucidated the structural and optical properties of the films. All the Raman spectra exhibited peaks characteristic of crystalline Cu<sub>2</sub>O.<sup>6</sup> In the PL spectra of the 2D and 3D Cu<sub>2</sub>O films, a near-band-edge emission peak was observed at 630 nm; the peak had a full width at half maximum (FWHM) of 15 nm and was not accompanied by emissions from deep levels. This peak is slightly blue-shifted from the band-edge emission of Cu<sub>2</sub>O, which is observed at approximately 640 nm; this was because of an emissive transition from an impurity donor band to the valence band.<sup>28</sup> The optical band gap was determined from the measured transmittance data using the conventional experimental/graphical method and found to be  $1.87 \text{ eV}$ , as shown in Fig. S3(d).

The reflectance spectra of the 2D and 3D Cu<sub>2</sub>O films are shown in Fig. S4 in the ESI. The dramatic decrease in the reflectance from 700

to 600 nm was related to the band gap energy of  $\text{Cu}_2\text{O}$ . In the infrared region, the reflectance of the 3D  $\text{Cu}_2\text{O}$  films was lower than that of the 2D  $\text{Cu}_2\text{O}$  films by 7–17%. Further, in the short-wavelength region (*i.e.*, for wavelengths of 350 to 600 nm), the reflectance of the 3D films was slightly lower than that of the 2D films. This suggests that light trapping occurred in the 3D films at all the wavelengths investigated in this study; this might be related to the random arrangement of the 3D structures. In particular, the reflectance of the 3D films in the near-infrared region was significantly lower than that of the 2D films. Furthermore, no light resonance was observed in the former as a result of scattering by their porous structure.

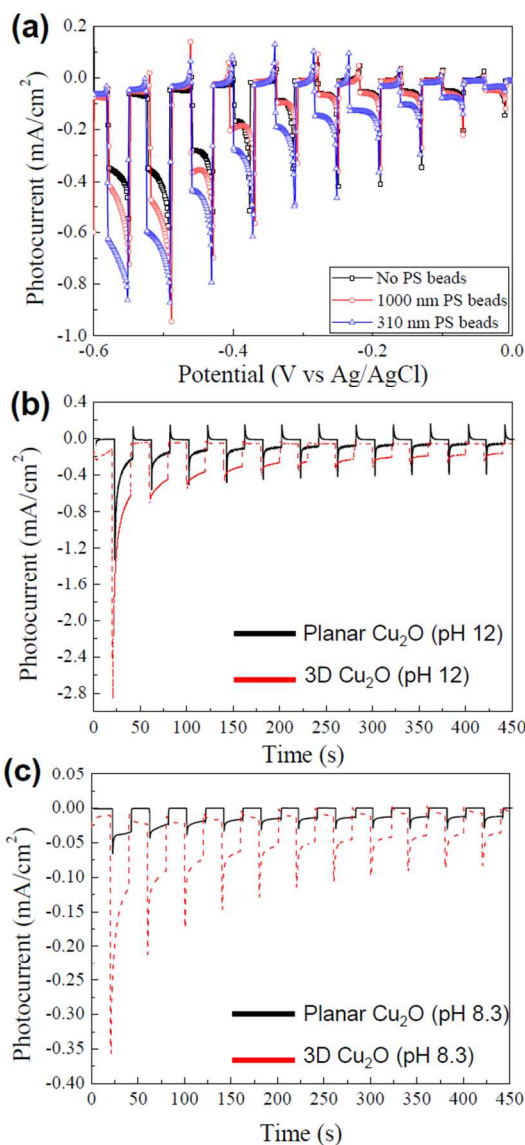


Figure 4. (a)  $I$ - $V$  characteristics of the 3D  $\text{Cu}_2\text{O}$  films deposited at pH 12 over the range  $-0.6$  to  $0$  V (*vs.* Ag/AgCl); the films were fabricated using templates of PS beads of different diameters. Also shown are the time-resolved photoresponses of the planar and 3D  $\text{Cu}_2\text{O}$  films deposited at (b) pH 12 and (c) pH 8.3, as measured in a  $0.5$  M  $\text{Na}_2\text{SO}_4$  solution at  $V = -0.4$  V (*vs.* Ag/AgCl).

The effect of the size of the PS beads used in the template on the photocurrent generated in the 3D films was investigated by templating the inverse-opal-structured  $\text{Cu}_2\text{O}$  films using beads with diameters of either 310 or 1000 nm. Figure 4(a) shows the  $I$ - $V$  curves for the resulting  $\text{Cu}_2\text{O}$  films; the curves were collected under chopped illumination. The photocurrent for the  $\text{Cu}_2\text{O}$  film fabricated using 300 nm PS beads was higher than that for the film obtained using 1000 nm beads. This implied that the latter film underwent reduction to a greater degree owing to its greater surface area. The spike observed during every light ON/OFF cycle was attributable to the preadsorbed water molecules on the films as well as to the electrolyte used.<sup>6</sup>

The photocurrents in the 3D films electrodeposited at pH 12 and 8.3 were both higher than those of the 2D films grown under the same conditions, as shown in Figs. 4(b) and (c). The intensity of the first photocurrent peak of the 3D film deposited at pH 12 was about twice that of the corresponding 2D film. The photocurrent decreased rapidly afterwards, as was also the case with the 2D film (Fig. 4 (b)). Similarly, the intensity of the first photocurrent peak of the 3D  $\text{Cu}_2\text{O}$  film deposited at pH 8.3 was 7 times higher than that of the corresponding planar film. The photocurrent then dropped significantly in the case of the 3D film (Fig. 4(c)), though such a change was not observed in the 2D film. The photocurrent was higher for the 3D films, owing to the randomly terminated layers on their surfaces and their porous structure. For this reason, the photocurrent of the 3D film deposited at pH 8.3 decreased significantly at the  $\text{O}_2^-$ -terminated layers. This decrease in the photocurrent was also confirmed on the basis of change in the colour of the film, which changed from red to black after the PEC analysis; a similar change was not observed in the case of the 2D film deposited at pH 8.3.

Even though the two 3D  $\text{Cu}_2\text{O}$  films consisted of randomly terminated layers, their electrical properties were different, as mentioned above. In particular, because of the low resistivity of the 3D film deposited at pH 12, its photocurrent ( $-0.25$  mA cm<sup>-2</sup> after 400 s) was higher than that of the 3D film deposited at pH 8.3 ( $-0.08$  mA cm<sup>-2</sup> after 400 s). If the exposed (100) facets of  $\text{Cu}_2\text{O}$  films have  $\text{O}^{2-}$ -terminated layers, reduction of the  $\text{Cu}_2\text{O}$  can result when the applied potential is less than the reduction potential of  $\text{Cu}_2\text{O}$  in dark conditions.<sup>16</sup> We found that the dark currents of the two 3D films were higher than those of the two 2D films; this was the result of the randomly terminated layers and larger surface areas of the 3D films. Because the reduction rate of  $\text{Cu}_2\text{O}$  at  $\text{O}^{2-}$ -terminated layers is higher under dark conditions, the 3D  $\text{Cu}_2\text{O}$  films had unstable surfaces, and the degradation of their photocurrents was accelerated.<sup>16</sup> However, the high photocurrent in the 3D  $\text{Cu}_2\text{O}$  films compared with the 2D films is not only caused by the reduction of  $\text{Cu}_2\text{O}$ , but also by  $\text{H}_2$  evolution. The generation of  $\text{H}_2$  by the 2D and 3D films deposited at pH 12 was compared. Because there is no passivation layer present, the amount of  $\text{H}_2$ , which was difficult to detect, is commonly generated at a bare  $\text{Cu}_2\text{O}$  film. However, after measurement in the PEC cell for 1 hr, a small amount of  $\text{H}_2$  was observed for a 3D  $\text{Cu}_2\text{O}$  sample (Fig S5 in the ESI). This is an indication that the increase in photocurrent is to the result of  $\text{H}_2$  generation. The surface of 3D

Cu<sub>2</sub>O films is more photoactive and better at producing H<sub>2</sub> than that of 2D films.

Table 1. PEC responses of the 2D and 3D Cu<sub>2</sub>O films deposited at different bath pH values.

Bath pH	Film structure	Initial photocurrent ( $I_0$ ) after 20 s <sup>a</sup> (mA cm <sup>-2</sup> )	Final photocurrent ( $I_f$ ) after 400 s <sup>a</sup> (mA cm <sup>-2</sup> )	$I_f/I_0$ after 400 s <sup>a</sup> (%)	Dark current <sup>a</sup> (mA cm <sup>-2</sup> )
12	Planar	-1.35	-0.39	28.9	-0.012
	3D <sup>b</sup>	-2.89	-0.25	8.7	-0.056
8.3	Planar	-0.07	-0.03	42.9	-0.0005
	3D <sup>b</sup>	-0.35	-0.08	22.9	-0.007

<sup>a</sup>Measured at -0.4 V (vs. Ag/AgCl).

<sup>b</sup>Deposited using the template of PS beads 310 nm in diameter.

Table 1 lists the photocatalytic characteristics of the Cu<sub>2</sub>O films deposited at different bath pH values and having different surface structures. The maximum values of the photocurrent were determined from the  $I-t$  curves collected at  $V = -0.4$  V (vs. Ag/AgCl). The 3D films exhibited greater degradation in  $I$  than did the 2D films; this was because of the larger surface area of the former. The 3D Cu<sub>2</sub>O films had randomly arranged planes that were exposed, and this resulted in significantly higher dark currents compared to the 2D films. The photocurrent degradation ratio of the 3D Cu<sub>2</sub>O films was 20% higher than that of the 2D Cu<sub>2</sub>O films, regardless of the bath pH during processing. As mentioned previously, this was a result of the fact that the surface area of the former films was higher, resulting in a higher effective reaction rate. The significant decrease in the photocurrent recorded for the 3D Cu<sub>2</sub>O films (91.3% for the film deposited at pH 12) will limit their application as photoelectrodes in PEC water-splitting cells. After the PEC cell measurements, the surface morphology of both the 2D and 3D Cu<sub>2</sub>O films was transformed to that of the leaf structure (Fig. S6 in the ESI). A Cu peak was observed in the XRD data collected after the PEC cell measurements lasting 1 hr because of Cu<sub>2</sub>O reduction (Fig. S7 in the ESI). The passivation of film surfaces to prevent degradation might be a good strategy for making such films suitable for use in 3D PEC water-splitting cells.

## Conclusions

We developed simple methods for manipulating the surface characteristics of Cu<sub>2</sub>O photoelectrodes. This was accomplished by electrodepositing the Cu<sub>2</sub>O films at different bath pH values and by depositing Cu<sub>2</sub>O films on templates of PS beads to create 3D surface structures with randomly arranged ion-terminated layers. The 2D/nontemplated Cu<sub>2</sub>O film deposited at pH 12 had a (111) orientation and exhibited a lower resistivity and higher photocurrent than those of the 2D film deposited at pH 8.3, which had a (100) orientation. The 3D films possessed several advantages over the 2D

ones, including larger surface areas and light absorption enhanced by light scattering. By combining the two surface manipulation techniques, a 3D Cu<sub>2</sub>O film electrodeposited at pH 12 on a template of PS beads 310 nm in diameter exhibiting an initial photocurrent of -2.8 mA cm<sup>-2</sup> was fabricated.

## Experimental

### Chemicals and materials

Copper(II) sulphate pentahydrate (CuSO<sub>4</sub>·5H<sub>2</sub>O; 99%), sodium citrate dihydrate (C<sub>6</sub>H<sub>5</sub>Na<sub>3</sub>O<sub>7</sub>·2H<sub>2</sub>O; 99%), Sodium sulphate, anhydrous (Na<sub>2</sub>SO<sub>4</sub>; 99%) and potassium hydroxide (KOH; 85%) were purchased from Daejung. Sodium lactic acid solution (CH<sub>3</sub>CH(OH)CO<sub>2</sub>H; 85%) was acquired from Aldrich. PS beads with diameters of 310 and 1000 nm were acquired from ThermoScientific.

### Fabrication of 2D and 3D Cu<sub>2</sub>O films

A schematic diagram of the process used to fabricate the 2D and 3D Cu<sub>2</sub>O films is shown in Fig. 5. A polar Cu<sub>2</sub>O film with exposed {100} surfaces was potentiostatically electrodeposited on an electron-beam-deposited Au(200 nm)/Ti(20 nm)/Si substrate using a mixture of 0.1 M copper sulphate, 1 M sodium citrate, and 4 M KOH as the electrolyte (pH = 12) at -0.3 V (vs. an Ag/AgCl reference electrode). A three-electrode system with a platinum plate as the counter electrode was employed for deposition. The temperature of the bath was maintained at 60 °C using a circulating chiller (Labkorea Inc., HLTC08). In addition, a nonpolar Cu<sub>2</sub>O film with exposed {111} surfaces was deposited at -0.4 V (vs. an Ag/AgCl reference electrode) using a solution of copper sulphate and lactic acid as the electrolyte<sup>4</sup> (pH = 8.3). These different bath conditions yielded different exposed surfaces. No impurities or other phases were observed during the XRD, Raman, or PL analyses. Therefore, the different bath condition did not influence any material factors save the nature of the exposed facets.

To deposit the inverse-opal-structured Cu<sub>2</sub>O films, a PS bead template was prepared on an Au/Ti/Si substrate using a solution of 2 mL ethanol and 50 μL of a commercial solution containing PS beads with diameters of either 310 or 1000 nm. The PS beads were randomly dispersed over the substrate by coating the substrate with the mixed solution and annealing it in an oven for 1–3 min at 80–140 °C to neck the PS beads.<sup>24</sup> The 3D Cu<sub>2</sub>O films then were synthesised on the PS template under the same conditions as for the 2D films. The PS beads were removed by immersing the films in chloroform for 3 hr. The charge density of the Cu<sub>2</sub>O films was fixed at 1 C cm<sup>-2</sup>. All the samples were annealed in air at 140 °C for 30 min to improve their crystallinity and electrical properties.<sup>4</sup> The thicknesses of both 3D sample and planar one are, on average, 3 μm

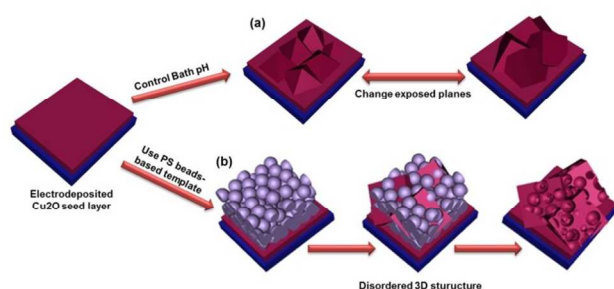


Figure 5. Schematic showing the surface manipulation methods investigated here: control of the bath pH and the use of a template of PS beads.

### Structural and electrical characterisation

The morphologies of the  $\text{Cu}_2\text{O}$  thin films were characterised using field-emission scanning electron microscopy (FESEM) (TESCAN, MIRA3). Their crystalline structures and preferred orientations were studied using X-ray diffractometry (XRD, Rigaku, D/MAX-2500/PC). The optical characteristics of the  $\text{Cu}_2\text{O}$  films were measured using an ultraviolet-visible spectrophotometer (PerkinElmer, Lambda 750). In addition, the Raman and photoluminescence (PL) spectra of the films were measured at room temperature using a Raman microscope (HORIBA, LabRam HR) with a 325 nm He-Cd laser. The electrical resistivities of the  $\text{Cu}_2\text{O}$  thin films, formed on Au/Ti-coated Si substrates, were hard to measure because of the high conductivities of the underlying metal layers. Therefore, the deposited films were detached from the substrates using an epoxy resin (Varian, TorrSeal). The electrical properties of the detached films could then be measured.<sup>25</sup> A tailor-made Hall Effect measurement unit in the van der Pauw configuration was employed for this purpose.

### Photoelectrochemical measurements

The PEC characteristics of the  $\text{Cu}_2\text{O}$  photoelectrodes were measured using 0.5 M sodium sulfate (pH 6.8) as the electrolyte.  $\text{O}_2$  was purged from the electrolyte by bubbling  $\text{N}_2$  into it under light illumination ( $125\text{mW cm}^{-2}$  halogen lamp). A platinum wire and an Ag/AgCl electrode were used as the counter and reference electrodes, respectively, in the three-electrode system. Linear sweep voltammetry was performed under light and in the dark for voltages ranging from 0 V to  $-0.6$  V (vs. Ag/AgCl); the scan rate was  $2\text{ mV s}^{-1}$ .

The time-dependent photocurrent responses of the photoelectrodes were measured under chopped light at  $-0.4$  V (vs. Ag/AgCl); the periods for which the light source was switched ON and OFF were both 20 s.  $\text{H}_2$  levels after illumination were analysed using a gas chromatograph with thermal conductivity detector (Hewlett Packard, HP6890). During the PEC cell measurements over the course of 1 hr, the electrolyte was bubbled with  $\text{N}_2$  gas to remove oxygen in the solution.

### Acknowledgements

This work was financially supported by New & Renewable Energy Grants from the Korea Institute of Energy Technology Evaluation and Planning (KETEP) (No. 20123010010160 and 20133030010890), funded by the Ministry of Trade, Industry and Energy, Korea, and by the Pioneer Research Centre Program of the National Research Foundation of Korea (2010-0002231), funded by the Ministry of Education, Science and Technology (MEST), Korea. Support was also provided by the Korean Institute of Materials Science.

### Notes and references

<sup>a</sup> Department of Materials Engineering, Hanyang University, Ansan-si, Gyeonggi-do 426-791, Republic of Korea.

<sup>b</sup> Electrochemistry Research Group, Materials Processing Division, Korea Institute of Materials Science, Changwon-si, Gyeongnam 641-831, Republic of Korea.

<sup>c</sup> Department of Metallurgical Engineering, Dong-A University, Busan-si, 426-791, Republic of Korea.

† To whom correspondence should be addressed: byyoo@hanyang.ac.kr, lim@kims.re.kr.

Electronic Supplementary Information (ESI) available: XRD patterns, Raman spectra, PL spectra, graphs of optical band gap, and reflectance spectra of the  $\text{Cu}_2\text{O}$  films. See DOI: 10.1039/b000000x/

- 1 M. Gratzel, *Nature*, 2001, **414**, 338-344.
- 2 O. Khaselev and J.A. Turner, *Science*, 1998, **280**, 425-427.
- 3 G.K. Mor, O.K. Varghese, R.H.T. Wilke, S. Sharma, K. Shankar, T.J. Latempa, K.S. Choi and C.A. Grimes, *NanoLett.*, 2008, **8**, 3555-3555.
- 4 A. Paracchino, V. Laporte, K. Sivula, M. Gratzel and E. Thimsen, *Nat. Mater.*, 2011, **10**, 456-461.
- 5 K.P. Musselman, A. Wisnet, D.C. Iza, H.C. Hesse, C. Scheu, J. L. MacManus-Driscoll and L. Schmidt-Mende, *Adv. Mater.*, 2010, **22**, E254-E258.
- 6 Y.C. Mao, J. T. He, X.F. Sun, W. Li, X. H. Lu, J.Y. Gan, Z.Q. Liu, L. Gong, J. Chen, P. Liu and Y.X. Tong, *Electrochim. Acta*, 2012, **62**, 1-7.
- 7 T. Mahalingam, J.S.P. Chitra, J.P. Chu, H. Moon, H. J. Kwon and Y.D. Kim, *J. Mater. Sci-Mater. Electron.*, 2006, **17**, 519-523.
- 8 N. Tetreault, E. Arsenaault, L.P. Heiniger, N. Soheilnia, J. Brillet, T. Moehl, S. Zakeeruddin, G.A. Ozin and M. Gratzel, *NanoLett.*, 2011, **11**, 4579-4584.
- 9 K.-S. Choi, *J. Phys. Chem. Lett.*, 2010, **1**, 2244-2250.
- 10 Y.G. Sun, C. H. Lei, D. Gosztola and R. Haasch, *Langmuir*, 2008, **24**, 11928-11934.
- 11 J.F. Chao, Z.R. Wang, X. Xu, Q. Y. Xiang, W.F. Song, G. Chen, J. B. Hu and D. Chen, *RSC Adv.*, 2013, **3**, 2746-2753.
- 12 S.K. Mohapatra, S. E. John, S. Banerjee and M. Misra, *Chem. Mater.*, 2009, **21**, 3048-3055.

## Journal Name

- 13 R. Tenne, *Nat. Nano.*, 2006, **1**, 103-111.
- 14 Y. Feldman, E. Wasserman, D.J. Srolovitz and R. Tenne, *Science*, 1995, **267**, 222-225.
- 15 Z.H. Li, J.W. Liu, D.J. Wang, Y. Gao and J. Shen, *Int. J. Hydrogen Energy*, 2012, **37**, 6431-6437.
- 16 K.L. Sowers and A. Fillinger, *J. Electrochem. Soc.*, 2009, **156**, F80-F85.
- 17 A. Paracchino, J.C. Brauer, J.E. Moser, E. Thimsen and M. Gratzel, *J. Phys. Chem. C*, 2012, **116**, 7341-7350.
- 18 A. Mittiga, E. Salza, F. Sarto, M. Tucci and R. Vasanthi, *Appl. Phys. Lett.*, 2006, **88**, 163502.
- 19 S.S. Jeong, A. Mittiga, E. Salza, A. Masci and S. Passerini, *Electrochim. Acta*, 2008, **53**, 2226-2231.
- 20 M. Izaki, T. Shinagawa, K.T. Mizuno, Y. Ida, M. Inaba and A. Tasaka, *J. Phys. D-Appl. Phys.*, 2007, **40**, 3326-3329.
- 21 L.C. Wang, N.R. de Tacconi, C.R. Chenthamarakshan, K. Rajeshwar and M. Tao, *Thin Solid Films*, 2007, **515**, 3090-3095.
- 22 C.M. McShane and K.S. Choi, *J. Am. Chem. Soc.*, 2009, **131**, 2561-2569.
- 23 E.C. Nelson, N.L. Dias, K.P. Bassett, S.N. Dunham, V. Verma, M. Miyake, P. Wiltzius, J.A. Rogers, J.J. Coleman, X.L. Li and P.V. Braun, *Nat. Mater.*, 2011, **10**, 676-681.
- 24 E.S. Kwak, W. Lee, N.G. Park, J. Kim and H. Lee, *Adv. Func. Mater.*, 2009, **19**, 1093-1099.
- 25 S. Yoon, I. Huh, J.H. Lim and B. Yoo, *Curr. Appl. Phys.*, 2012, **12**, 784-788.
- 26 J.A. Switzer, H.M. Kothari, E.W. Bohannon, *J. Phys. Chem. B*, 2002, **106**, 4027-4031.
- 27 R. Liu, F. Oba, E.W. Bohannon, F. Ernst and J.A. Switzer, *Chem. Mater.*, 2003, **15**, 4882-4885.
- 28 K. Mizuno, M. Izaki, K. Murase, M. Chigane, M. Inaba, A. Tasaka and Y. Awakura, *J. Electrochem. Soc.*, 2005, **152**, C179-C182.